Eur. Phys. J. C (2022) 82:168
https://doi.org/10.1140/epjc/s10052-022-10102-9

THE EUROPEAN PHYSICAL JOURNAL C

Regular Article - Experimental Physics

Study of the process $e^+e^- \to \eta\eta\gamma$ in the energy range $\sqrt{s} = 1.17$–2.00 GeV with the SND detector

SND Collaboration

M. N. Achasov[1,2], A. Yu. Barnyakov[1,2], K. I. Beloborodov[1,2], A. V. Berdyugin[1,2], D. E. Berkaev[1,2], A. G. Bogdanchikov[1], A. A. Botov[1], T. V. Dimova[1,2], V. P. Druzhinin[1,2], A. N. Kirpotin[1], L. V. Kardapoltsev[1,2,a], A. S. Kasaev[1], A. G. Kharlamov[1,2], I. A. Koop[1,2], A. A. Korol[1,2], D. P. Kovrizhin[1], A. S. Kupich[1,2], K. A. Martin[1], N. A. Melnikova[1], N. Yu. Muchnoy[1,2], A. E. Obrazovsky[1], E. V. Pakhtusova[1], K. V. Pugachev[1,2], D. V. Rabusov[1], Yu. A. Rogovsky[1,2], A. I. Senchenko[1,2], S. I. Serednyakov[1,2], D. N. Shatilov[1], Yu. M. Shatunov[1,2], D. A. Shtol[1], D. B. Shwartz[1,2], Z. K. Silagadze[1,2], I. K. Surin[1], M. V. Timoshenko[1], Yu. V. Usov[1], V. N. Zhabin[1], V. V. Zhulanov[1,2]

[1] Budker Institute of Nuclear Physics, SB RAS, Novosibirsk 630090, Russia
[2] Novosibirsk State University, Novosibirsk 630090, Russia

Received: 15 October 2021 / Accepted: 5 February 2022 / Published online: 23 February 2022

Abstract The process $e^+e^- \to \eta\eta\gamma$ is studied in the center-of-mass energy range 1.17–2.00 GeV using data with an integrated luminosity of 201 pb^{-1} collected by the SND detector at the VEPP-2000 e^+e^- collider. The $e^+e^- \to \eta\eta\gamma$ cross section is measured for the first time. It is shown that the dominant mechanism of this reaction is the transition through the $\phi\eta$ intermediate state. Our result on the $e^+e^- \to \eta\eta\gamma$ cross section is consistent with the $e^+e^- \to \phi\eta$ measurement in the $\phi \to K^+K^-$ mode. The search for radiative processes contributing to the $e^+e^- \to \eta\eta\gamma$ cross section is performed, and no significant signal is observed.

1 Introduction

This work is devoted to study of the process

$$e^+e^- \to \eta\eta\gamma \tag{1}$$

in the center-of-mass (c.m.) energy range $\sqrt{s} = 1.17$–2.00 GeV at the experiment with the SND detector at the VEPP-2000 e^+e^- collider. Previously, this process was studied only near the J/ψ resonance by the Crystal Ball [1] and BESIII [2] collaborations.

The dominant contribution to the $e^+e^- \to \eta\eta\gamma$ cross section in the energy region under study comes from the process $e^+e^- \to \phi\eta$ with the decay $\phi \to \eta\gamma$. This process was well studied in the SND [3], CMD-3 [4], BABAR [5,6] and BESIII [7] experiments in the decay channel $\phi \to K^+K^-$. In this work, the main objective of the analysis is the search of other intermediate states. In addition to the known $\rho\eta$ and $\omega\eta$ mechanisms, the most probable are radiative decays of excited vector mesons into $f_0(1500)\gamma$ and $f_2'(1525)\gamma$. Measuring the widths of these decays is important for understanding of the quark structure of excited light vector mesons. In particular, there are indications that the excited states of ρ and ω mesons can be a mixture of $q\bar{q}$ and vector hybrid states [8]. The widths of radiative decays of excited vector mesons are sensitive to the hybrid state admixture [9].

In Ref. [9], the decay width of $\phi(1680) \to f_2'(1525)\gamma$ was calculated within the framework of the quark model. For the $\rho(1700) \to f_0(1500)\gamma$ channel the additional assumption was used that the states $f_0(1370)$, $f_0(1500)$, and $f_0(1710)$ are a mixture of states from light quarks and a glueball. It was shown that the width of this decay strongly depends on the glueball mass. The total cross section for the production of resonances $\phi(1680)$ and $\rho(1700)$ in e^+e^- collisions can be estimated as 11 and 15 nb, respectively. Using results of Ref. [9] and the branching ratios $B(f_2'(1525) \to \eta\eta) = 11.6 \pm 2.2\%$ and $B(f_0(1500) \to \eta\eta) = 6.0 \pm 0.9\%$ [10] we obtain the following estimates for the cross sections at the maxima of the resonances $\rho(1700)$ and $\phi(1680)$:

$$\sigma(e^+e^- \to f_2'(1525)\gamma \to \eta\eta\gamma) \approx 1.7\text{pb}, \tag{2}$$

$$\sigma(e^+e^- \to f_0(1500)\gamma \to \eta\eta\gamma) \approx 0.4\text{–}1.9\ \text{pb}. \tag{3}$$

These cross sections are small compared to the cross section for the $\phi\eta$ intermediate state, which is about 35 pb at $\sqrt{s} = 1.68$ GeV.

[a] email: l.v.kardapoltsev@inp.nsk.su (corresponding author)

2 Detector and experiment

SND is a general-purpose non-magnetic detector [11–14] collecting data at the VEPP-2000 e^+e^- collider [15]. Its main part is a three-layer spherical electromagnetic calorimeter consisting of 1630 NaI(Tl) crystals. The calorimeter covers a solid angle of 95% of 4π. The energy resolution of the calorimeter for photons is $\sigma_E/E = 4.2\%/\sqrt[4]{E(\text{GeV})}$. The angular resolution is about 1.5°. Directions of charged particles are measured using a nine-layer drift chamber and one-layer proportional chamber in a common gas volume. The solid angle of the tracking system is 94% of 4π. A system of threshold aerogel Cherenkov counters located between the tracking system and the calorimeter is used for charged kaon identification. Outside the calorimeter, a muon detector consisting of proportional tubes and scintillation counters is placed.

Monte-Carlo (MC) simulation of the signal and background processes takes into account radiative corrections [16]. The angular distribution of hard photon emitted from the initial state is generated according to Ref. [17]. Interactions of the particles produced in e^+e^- annihilation with the detector materials are simulated using the GEANT4 software [18]. The simulation takes into account variation of experimental conditions during data taking, in particular dead detector channels and beam-induced background. To take into account the effect of superimposing the beam background on the e^+e^- annihilation events, simulation uses special background events recorded during data taking with a random trigger. These events are superimposed on simulated events, leading to the appearance of additional tracks and photons.

The analysis presented in this work is based on data with an integrated luminosity of 201 pb^{-1} recorded in 2010–2020. These data were collected at 138 energy points in the energy region $\sqrt{s} = 1.17$–2.00 GeV. Since the cross section of the process under study is small, for the convenience of analysis, the data are combined into 6 energy intervals listed in Table 1.

The process $e^+e^- \to \eta\eta\gamma$ is studied in the five-photon final state. Since there are no charged particles in the final state of the process under study, it is viable to use the process $e^+e^- \to \gamma\gamma$ for normalization. As a result of the normalization a part of systematic uncertainties associated with the hardware event selection and beam-induced background is canceled out. Accuracy of the luminosity measurement using the process $e^+e^- \to \gamma\gamma$ is estimated to be 2% [19].

3 Event selection

Selection of $e^+e^- \to \eta\eta\gamma \to 5\gamma$ events is performed in two stages. At the first stage, we select events with exactly 5 photons with energies above 20 MeV and no charged tracks. The latter condition is ensured by requiring that the number of hits in the drift chamber is less than four. The transverse profile of energy deposition in the calorimeter for reconstructed photons must be consistent with the expected distribution for electromagnetic shower [20]. To suppress cosmic-ray background, absence of a signal in the muon system is required. The following conditions provides an approximate balance of energy and momentum in an event:

$$E_{\text{EMC}}/\sqrt{s} > 0.6,\ P_{\text{EMC}}/\sqrt{s} < 0.3, \tag{4}$$

where E_{EMC} is the total energy deposition in the calorimeter, and P_{EMC} is the total event momentum calculated using energy depositions in calorimeter crystals.

The main background processes are

$$e^+e^- \to \omega\pi^0 \to \pi^0\pi^0\gamma, \tag{5}$$

and

$$e^+e^- \to \omega\eta \to \eta\pi^0\gamma. \tag{6}$$

We also study background from the following reactions with multiphoton final states:

$$\begin{aligned} &e^+e^- \to \omega\pi^0\pi^0 \to \pi^0\pi^0\pi^0\gamma, \\ &e^+e^- \to \omega\eta\pi^0 \to \eta\pi^0\pi^0\gamma, \end{aligned} \tag{7}$$

and from the QED processes

$$e^+e^- \to 4\gamma, 5\gamma. \tag{8}$$

Additional photons in the process $e^+e^- \to 4\gamma$ arise from the splitting of electromagnetic showers, and the beam-induced background.

To suppress background from the processes listed above, a kinematic fits are performed to the hypotheses $e^+e^- \to 5\gamma$, $e^+e^- \to \pi^0\pi^0\gamma$, $e^+e^- \to \eta\pi^0\gamma$, and $e^+e^- \to \eta\eta\gamma$ with the requirements of energy and momentum balance in an event. For the hypotheses with final states $\pi^0\pi^0\gamma$, $\eta\pi^0\gamma$, and $\eta\eta\gamma$, the additional constraints are imposed that the invariant masses of photon pairs are equal to the masses of the π^0 and η mesons. As a result of the kinematic fit, the energies and angles of photons are refined, and the χ^2 of the proposed kinematic hypothesis is calculated. In the kinematic fits, all possible combinations of photons are tested, and the combination with the smallest χ^2 value is retained. The following conditions are applied to the obtained χ^2 values

$$\chi^2_{\eta\eta\gamma} - \chi^2_{5\gamma} < 60, \quad \chi^2_{5\gamma} < 30, \quad \chi^2_{\pi^0\pi^0\gamma} - \chi^2_{5\gamma} > 100. \tag{9}$$

To suppress the $e^+e^- \to \eta\pi^0\gamma$ background, the condition

$$\chi^2_{\eta\pi^0\gamma} - \chi^2_{5\gamma} > 30 \tag{10}$$

is imposed. This background source is important only above the $\omega\eta$ production threshold [19]. Therefore, the condition (10) is not applied for events from the first energy interval (see Table 1), at $\sqrt{s}$ <1.32 GeV. Using the criteria described above, 183 data events are selected for further analysis.

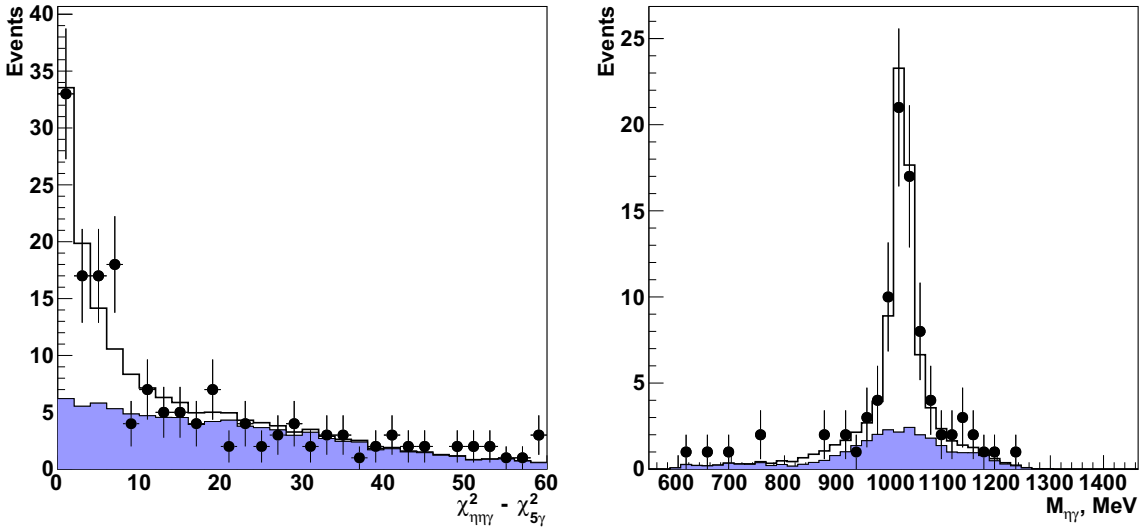

Fig. 1 Left panel: The $\chi^2_{\eta\eta\gamma} - \chi^2_{5\gamma}$ distribution for selected data events with $\sqrt{s} = 1.57$–2.00 GeV (points with error bars). The solid histogram is the result of the fit with the sum of the signal and background distributions described in the text. The shaded histogram represents the background distribution. Right panel: The distribution of $M_{\eta\gamma}$ closest to the ϕ meson mass for data events with $\sqrt{s} = 1.57$–2.00 GeV selected with the tighter condition $\chi^2_{\eta\eta\gamma} - \chi^2_{5\gamma} < 10$ (points with error bars). The solid histogram is the simulated signal plus background distribution calculated with the fitted numbers of signal and background events. The shaded histogram is the simulated background distribution

4 Fitting the $\chi^2_{\eta\eta\gamma} - \chi^2_{5\gamma}$ distribution

The $\chi^2_{\eta\eta\gamma} - \chi^2_{5\gamma}$ distribution for selected data events from the energy range $\sqrt{s} = 1.57$–2.00 GeV is shown in Fig. 1 (left). To determine the number of $\eta\eta\gamma$ events, this distribution is fitted with the sum of signal and background distributions.

The signal distribution is obtained using MC simulation as a sum of the distributions for the processes

$$e^+e^- \to \phi\eta, \quad e^+e^- \to \rho\eta, \quad e^+e^- \to \omega\eta \tag{11}$$

with the subsequent decays of the vector mesons to $\eta\gamma$. The interference between these processes is neglected in the sum. The total number of signal events is a free fit parameter. The fractions of the processes (11) in the sum are calculated using their measured cross sections [4,21,22] and the branching fractions of the decays $\phi, \rho, \omega \to \eta\gamma$ [10]. The energy dependences of the cross sections for the processes (11) are shown in Fig. 2.

Imperfect simulation of the detector response may lead to difference between data and simulation in the $\chi^2_{\eta\eta\gamma} - \chi^2_{5\gamma}$ distribution. To study this effect, we use events of the process $e^+e^- \to \pi^0\pi^0\gamma$ from the energy region $\sqrt{s} = 1.05$–1.7 GeV, where they are selected practically without background. For these events, the distribution of the parameter $\chi^2_{\pi^0\pi^0\gamma} - \chi^2_{5\gamma}$ is studied. The parameters $\chi^2_{\eta\eta\gamma}$ and $\chi^2_{\pi^0\pi^0\gamma}$ are calculated using the kinematic fits with the same number of constraints, differing only in the masses of intermediate particles. Although the photon spectra in $\eta\eta\gamma$ and $\pi^0\pi^0\gamma$ events are different, we expect that the correction to the $\chi^2_{\pi^0\pi^0\gamma} - \chi^2_{5\gamma}$ distribution is close to the correction to the $\chi^2_{\eta\eta\gamma} - \chi^2_{5\gamma}$ distribution. It turned out that the difference between data and simulation can be described by stretching the simulated distribution. To find the stretching parameter α_b, the data distribution is fitted by the simulated distribution of the parameter $\alpha_b(\chi^2_{\pi^0\pi^0\gamma} - \chi^2_{5\gamma})$. The resulting value $\alpha_b = 1.05 \pm 0.01$ allows to match well the distributions for data and simulation. In particular, χ^2/ndf changes from 49/29 at $\alpha_b = 1$ to 34/28 at $\alpha_b = 1.05$, where ndf is the number of degrees of freedom. This correction is applied to the $\chi^2_{\eta\eta\gamma} - \chi^2_{5\gamma}$ distribution obtained from simulation. To estimate the associated systematic uncertainty, α_b is treated in the fit as a nuisance parameter with a Gaussian distribution, the standard deviation of which is conservatively estimated to be 0.05.

For description of the background distribution, the processes (5)–(8) are taken into account. Other multiphoton processes make a negligible contribution. The total number of background events is a free fit parameter, while the relative contributions (β_i) of the different processes are calculated using their measured cross sections. Since the $\chi^2_{\eta\eta\gamma} - \chi^2_{5\gamma}$ distributions for different background processes ($P_{\mathrm{bkg,i}}$) are slightly different, the uncertainties in β_i lead to an uncertainty in background subtraction. To estimate this uncertainty, the background distribution used in the fit is presented as a sum $\sum_i \beta_i P_{\mathrm{bkg,i}}$. The parameters β_i are treated as nuisance parameters with Gaussian constraints.

The result of the fit to the $\chi^2_{\eta\eta\gamma} - \chi^2_{5\gamma}$ distribution for data events from the energy range $\sqrt{s} = 1.57$–2.00 GeV is shown in Fig. 1 (left). The following values are obtained for

the numbers of the signal and background events

$$N_{\eta\eta\gamma} = 69.7 \pm 12.0, \quad N_{\rm bkg} = 91.3 \pm 12.9. \tag{12}$$

The quoted errors are statistical. The systematic uncertainty in the number of signal events due to the uncertainty in α_b is 3%. The uncertainty due to the variation of the β_i coefficients is 1%. The total contribution from background processes (5)–(7) calculated using their measured cross sections and the detection efficiencies obtained from simulation is $N^{\rm exp}_{\rm bkg} = 81.4 \pm 4.3$. The same number for the signal processes (11) is $N^{\rm exp}_{\eta\eta\gamma} = 73.5 \pm 3.5$. Both numbers are in good agreement with the results of the fit.

Figure 1 shows the distribution of the $\eta\gamma$ invariant mass ($M_{\eta\gamma}$) closest to the ϕ meson mass for data events from the energy range $\sqrt{s} = 1.57$–2.00 GeV selected with the tighter condition $\chi^2_{\eta\eta\gamma} - \chi^2_{5\gamma} < 10$. The solid histogram represents the expected $M_{\eta\gamma}$ distribution for the fitted numbers of the $\eta\eta\gamma$ and background events . It is seen that our model describes the data distribution well. The clear peak at the ϕ meson mass corresponds to the dominant $\phi\eta$ intermediate mechanism.

The fit described above is performed in 6 energy intervals. The results are listed in Table 1. For the second energy interval, the fitted number of signal events is negative. negative number of events is allowed in the fit to obtain a correct estimate of the statistical uncertainty. Using the profile likelihood method [23] with a prior function that is uniform in the physical region $\sigma > 0$ the upper limits on the cross section are calculated for the first two energy intervals.

5 Detection efficiency and radiative corrections

The Born cross section averaged over the energy interval is calculated as follows

$$\sigma = \frac{N_{\eta\eta\gamma}}{L\varepsilon(1+\delta)}, \tag{13}$$

where $L = \sum_i L_i$ is the total integrated luminosity for the interval, L_i is the integrated luminosity at the ith energy point within the interval, ε and δ are the detection efficiency and radiative correction averaged over the interval. To calculate ε and δ, it is necessary to know relations between different intermediate mechanisms of the process $e^+e^- \to \eta\eta\gamma$ and the energy dependence of the cross section for each of the mechanisms. We assume that the intermediate mechanisms $\phi\eta$, $\omega\eta$ and $\rho\eta$ make the dominant contribution to the cross section of the process under study. The Born cross section calculated as the sum of the contributions of these mechanisms is shown in Fig. 2. The calculation is based on the approximation of the experimental data [4,21,22].

Above 1.6 GeV, the main contribution to the cross section arises from the $\phi\eta$ mechanism, while below 1.6 GeV, the dominant mechanism is $\rho\eta$. In the sum, we neglect the interference between the amplitudes of the intermediate states. The highest interference is expected between amplitudes $\rho\eta$ and $\omega\eta$. Its value depends on the relative phase between the amplitudes. We estimate that at 1.5 GeV the maximum value of the interference contribution to the cross section can reach 30%. At 1.65 GeV, the interference contribution does not exceed 1%.

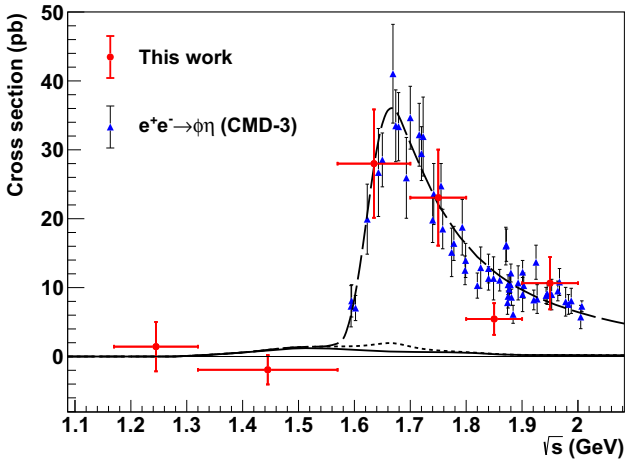

Fig. 2 The the $e^+e^- \to \eta\eta\gamma$ Born cross section measured in this work (circles) compared with the $e^+e^- \to \phi\eta$ cross section measured by CMD-3 in the decay mode $\phi \to K^+K^-$ [4] multiplied by the branching fraction of the decay $\phi \to \eta\gamma$ (triangles). The solid curve is the $e^+e^- \to \rho\eta$ cross section, the dotted curve is the sum of the $e^+e^- \to \rho\eta$ and $\omega\eta$ cross sections, while the dashed line is the sum of the $e^+e^- \to \phi\eta$, $\rho\eta$ and $\omega\eta$ cross sections

For each energy point i and each reaction mechanism j we calculate the visible cross section

$$\sigma_{vis,j}(s_i) = \int_0^{x_{max}} F(x, s_i)\sigma_j(s_i(1-x))dx, \tag{14}$$

where $F(x, s_i)$ is a so-called radiator function [16] describing the distribution of the energy fraction $x = E_r/2\sqrt{s}$ carried away by photons emitted from the initial state, and $\sigma_j(s)$ is the Born cross section for jth mechanism.

The detection efficiency and radiative correction averaged over the energy interval are calculated as

$$\varepsilon = \sum_{i,j} \varepsilon_{i,j} L_i \sigma_{vis,j}(s_i) \Big/ \sum_{i,j} L_i \sigma_{vis,j}(s_i), \tag{15}$$

$$1 + \delta = \sum_{i,j} L_i \sigma_{vis,j}(s_i) \Big/ \sum_{i,j} L_i \sigma_j(s_i), \tag{16}$$

where $\varepsilon_{i,j}$ is the detection efficiency calculated using simulation for the jth intermediate mechanism at the ith energy point. The obtained values of ε and $(1+\delta)$ are listed in Table 1.

To estimate the model dependence of the measured cross section, the $\phi\eta$, $\omega\eta$ and $\rho\eta$ contributions in Eqs. (15) and (16)

Table 1 The energy range ($\sqrt{s}$), integrated luminosity (L), detection efficiency (ε), number of signal ($N_{\eta\eta\gamma}$) and background ($N_{\rm bkg}$) events obtained from the fit, number of expected background events ($N_{\rm bkg}^{\rm exp}$), radiative correction ($1+\delta$) and Born cross section (σ) for the process $e^+e^- \to \eta\eta\gamma$. The quoted errors are statistical. For the first two energy ranges, the 90% confidence level upper limits on the cross section are given in parentheses. The systematic uncertainty in the cross section is 21% for $\sqrt{s} < 1.32$ GeV, 23% for $1.32 < \sqrt{s} < 1.57$ GeV, and 12% for $\sqrt{s} > 1.57$ GeV

$\sqrt{s}$, GeV	L, pb^{-1}	ε, %	$N_{\eta\eta\gamma}$	$N_{\rm bkg}$	$N_{\rm bkg}^{\rm exp}$	$1+\delta$	σ, pb
1.17–1.32	26.0	4.81	1.4 ± 3.4	17.6 ± 5.2	16.9 ± 0.9	0.754	1.4 ± 3.6 (< 6.8)
1.32–1.57	27.4	3.10	-1.4 ± 1.6	3.9 ± 1.8	9.6 ± 0.4	0.881	-1.9 ± 2.1 (< 2.5)
1.57–1.70	19.3	4.06	18.8 ± 5.3	13.2 ± 4.7	12.0 ± 0.7	0.857	28.0 ± 7.9
1.70–1.80	15.8	4.18	14.8 ± 4.5	6.2 ± 3.4	8.6 ± 0.7	0.972	23.0 ± 7.0
1.80–1.90	65.6	3.84	14.6 ± 6.2	39.4 ± 7.9	35.9 ± 4.7	1.062	5.4 ± 2.3
1.90–2.00	46.8	3.83	20.9 ± 7.4	33.1 ± 8.2	25.0 ± 4.5	1.095	10.6 ± 3.8

are varied within their experimental errors. To determine the uncertainty associated with the interference between the $\omega\eta$ and $\rho\eta$ mechanisms, we increased/decreased the $\omega\eta$ contribution by the value of the interference term between the $\omega\eta$ and $\rho\eta$ amplitudes. The efficiency is weakly dependent on the intermediate mechanism. Therefore, when calculating the efficiency, we assume that the efficiency for events corresponding to the interference term is close to the efficiency for $\omega\eta$ events. We also added to the sums (15) and (16) terms corresponding to the mechanisms $f_0(1500)\gamma$ or $f_2'(1525)\gamma$ with cross sections equal to the upper limits set in Sect. 6. The model uncertainty in the $e^+e^- \to \eta\eta\gamma$ cross section determined in this way does not exceed 2% for $\sqrt{s} > 1.57$ GeV and 20% for $\sqrt{s} < 1.57$ GeV.

Imperfect simulation of the detector response leads to a systematic uncertainty in the detection efficiency obtained using the simulation. The difference between data and simulation in the distributions of χ^2 of kinematic fits for the process $e^+e^- \to \omega\pi^0 \to \pi^0\pi^0\gamma$ were studied using large statistics in Refs. [24,25]. Based on this study, we conclude that the systematic uncertainty due to the conditions (9) does not exceed 5%. The condition $\chi^2_{\eta\pi\gamma} - \chi^2_{5\gamma} > 30$, specific for this analysis, reduces the detection efficiency by approximately 2 times. To determine the efficiency correction associated with this condition, its boundary is varied from 30 to 10. The observed variation of the measured cross section is 1.01 ± 0.10. Thus, no additional efficiency correction is introduced, and the error of the obtained correction 10% is taken as an estimate of the systematic uncertainty due to condition (10). The total systematic uncertainty of the detection efficiency due to the selection conditions is 11% for $\sqrt{s} > 1.32$ GeV and 5% for $\sqrt{s} < 1.32$ GeV.

In SND, photons converting into a e^+e^- pair in the material before the drift chamber, produce a charged track. Such events do not pass the selection criteria. Since the process under study and the process used for normalization contain different numbers of photons in the final state, improper simulation of the photon conversion lead to a shift in the measured cross section. The photon conversion probability is measured using events of the process $e^+e^- \to \gamma\gamma$. The corresponding efficiency correction is found to be $(-0.79 \pm 0.02)\%$.

Table 2 The main sources of the systematic uncertainty in the measured $e^+e^- \to \eta\eta\gamma$ cross section

Source	
Luminosity	2%
Selection conditions	5–11%
Background subtraction	1%
$\chi^2_{\eta\eta\gamma} - \chi^2_{5\gamma}$ distribution shape	3%
Model dependence	2–20%
Total	12–23%

The values of the $e^+e^- \to \eta\eta\gamma$ Born cross section for six energy intervals obtained using Eq. (13) are listed in Table 1. In Fig. 2, the measured cross section is compared with the calculation for the mechanisms $\phi\eta$, $\omega\eta$ and $\rho\eta$ based on the approximation of the experimental data [4,21,22]. Figure 2 also shows the measurement of the cross section for the dominant mechanism $e^+e^- \to \phi\eta$ performed by CMD-3 in decay mode $\phi \to K^+K^-$ [4]. It is seen that our results agree with both the calculation and the CMD-3 measurement.

Only statistical errors are quoted in Table 1 and Fig. 2. The systematic uncertainty is 21% for $\sqrt{s} < 1.32$ GeV, 23% for $1.32 < \sqrt{s} < 1.57$ GeV, and 12% for $\sqrt{s} > 1.57$ GeV. The sources of the systematic uncertainty are listed in Table 2.

6 Search for radiative processes

It is interesting to search for intermediate mechanisms of the $e^+e^- \to \eta\eta\gamma$ reaction other than $\phi\eta$, $\omega\eta$, and $\rho\eta$. The most likely additional mechanisms are $f_0(1500)\gamma$ and $f_2'(1525)\gamma$. To increase the sensitivity to them, it is required to suppress the contribution of the dominant mechanism $\phi\eta$. For this,

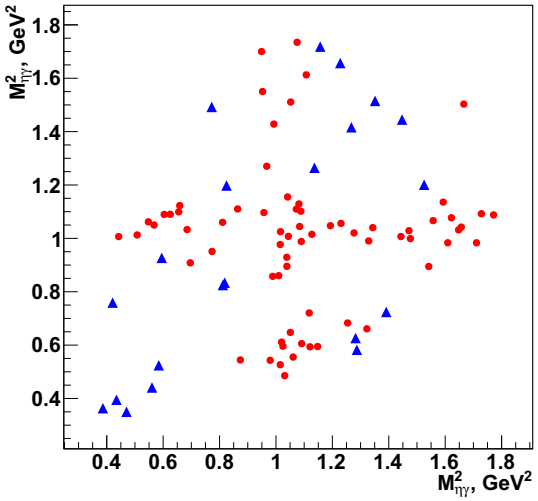

Fig. 3 The scatter plot of the two $\eta\gamma$ invariant mass squared combinations for data events with $\sqrt{s} = 1.57$–2.00 GeV selected with the condition $\chi^2_{\eta\eta\gamma} - \chi^2_{5\gamma} < 10$. Events that satisfy the condition $\chi^2_{\phi\eta} - \chi^2_{\eta\eta\gamma} > 20$ are marked by blue triangles

an additional kinematic fit is performed to the hypothesis $e^+e^- \to \phi\eta \to \eta\eta\gamma$, in which the constraint is added that one of the two invariant masses of the $\eta\gamma$ system is equal to the ϕ meson mass. The following condition is imposed on the χ^2 of the kinematic fit:

$$\chi^2_{\phi\eta} - \chi^2_{\eta\eta\gamma} > 20. \tag{17}$$

Figure 3 shows the scatter plot of the two $\eta\gamma$ invariant mass combinations for data events with $\sqrt{s} = 1.57$–2.00 GeV. Events of the $e^+e^- \to \phi\eta$ process form bands around $m^2_{\eta\gamma} \approx 1$ GeV^2. Events that satisfy the condition (17) are marked by blue triangles. It is seen that several events with $\chi^2_{\phi\eta} - \chi^2_{\eta\eta\gamma} < 20$ have the $\eta\gamma$ masses that are vary different from the ϕ mass. In these events $\chi^2_{\eta\eta\gamma}$ for the wrong combination of photons has a smaller value than for the correct one. For this reason, the condition (17) suppresses $\phi\eta$ events more effectively than cuts on $m_{\eta\gamma}$'s. It rejects about 90% of $e^+e^- \to \phi\eta$ events. At the same time, the detection efficiency for the processes $e^+e^- \to f_0(1500)\gamma$ and $f_2'(1525)\gamma$ decreases only by a factor of about 2. The number of selected events in the entire energy range decreases to 86 after applying the condition (17). The $\chi^2_{\eta\eta\gamma} - \chi^2_{5\gamma}$ distribution for data events from the energy region $\sqrt{s} = 1.57$ - 2.00 GeV is shown in Fig. 4 (left). The distribution of the $\eta\eta$ invariant mass for data events with $\chi^2_{\eta\eta\gamma} - \chi^2_{5\gamma} < 10$ is shown in Fig. 4 (right). It is seen that the data distributions is well described by the expected distribution for the background processes (5)–(8) and the processes (11).

Since no significant signal from radiative processes is observed, we set upper limits on their cross sections. To do this, we compare the data $\chi^2_{\eta\eta\gamma} - \chi^2_{5\gamma}$ distribution with the same distributions for signal and background, using the CL_s technique [26,27].

As input, the procedure [27] requires the measured distribution, the distributions for signal and background, the expected number of background events, and the systematic uncertainties for the signal and background. The systematic uncertainties due to the luminosity measurement, selection

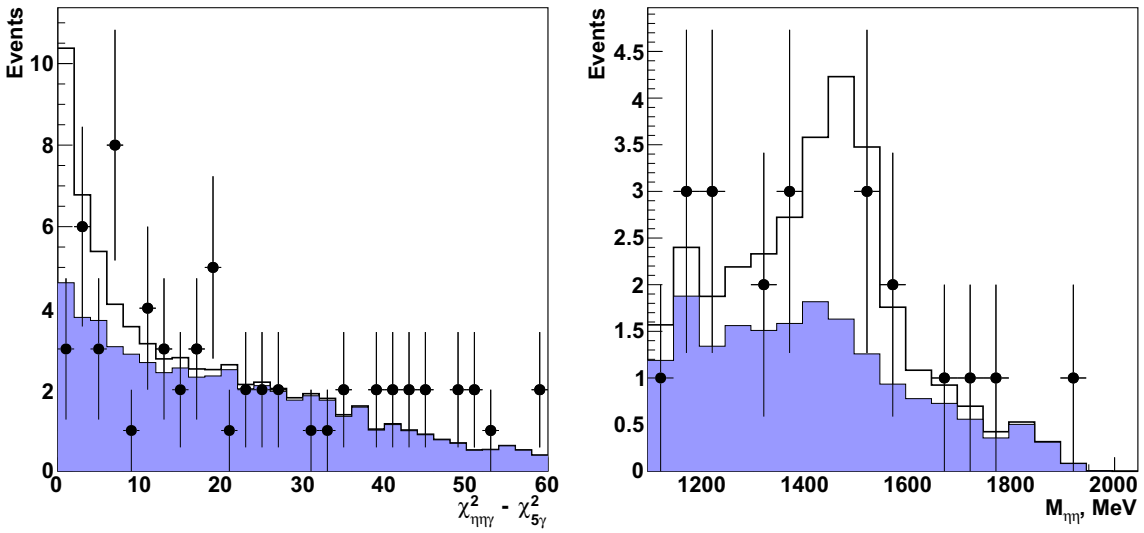

Fig. 4 The $\chi^2_{\eta\eta\gamma} - \chi^2_{5\gamma}$ (left panel) and $M_{\eta\eta}$ distributions for data events from the energy region $\sqrt{s} = 1.57$–2.00 GeV selected with the additional condition $\chi^2_{\phi\eta} - \chi^2_{\eta\eta\gamma} > 20$ (points with error bars). For the $M_{\eta\eta}$ distribution, events are selected with the tighter condition $\chi^2_{\eta\eta\gamma} - \chi^2_{5\gamma} < 10$. The shaded histogram is the expected distribution for the background processes (5)–(8) and the processes (11). The solid histogram is the sum of the shaded distribution and the distribution for events of the process $e^+e^- \to f_0(1500)\gamma \to \eta\eta\gamma$ with a cross section of 5 pb

Table 3 The energy range ($\sqrt{s}$), integrated luminosity (L), detection efficiency (ε), 90% CL upper limit on number of events of radiative processes (N_{rad}), number of expected background events ($N_{\rm bkg}^{\rm exp}$), radiative correction ($1+\delta$), 90% CL upper limit on the Born cross section for the radiative processes (σ)

$\sqrt{s}$, GeV	L, pb^{-1}	ε, %	N_{rad}	$N_{\rm bkg}^{\rm exp}$	$1+\delta$	σ, pb
1.17–1.32	26.0	4.28	7.0	16.9 ± 0.9	0.915	6.8
1.32–1.57	27.4	2.60	2.5	10.3 ± 0.4	0.964	3.7
1.57–1.80	35.1	2.03	7.5	17.8 ± 0.7	0.982	10.7
1.80–2.00	112.4	2.04	7.7	37.4 ± 3.5	0.989	3.4

criteria, and imperfect simulation of the $\chi^2_{\eta\eta\gamma} - \chi^2_{5\gamma}$ distribution are similar to those listed in Table 2. To estimate the expected number of background events, we use the measured cross sections for the background processes and the detection efficiencies obtained using simulation. In this case, background processes are not only the processes (5)–(8), but also (11).

The estimation of the systematic uncertainty in the expected number of background events is performed under assumption that it is completely determined by the experimental accuracy of the measured cross sections for the background processes. The detection efficiency for signal events is calculated as a half sum of the efficiencies for $e^+e^- \to f_0(1500)\gamma$ and $f_2'(1525)\gamma$ events. Their half difference is used as an estimate of the model dependence of the detection efficiency. It does not exceed 6%.

To average the efficiency and radiative correction in Eqs. (15) and (16), we use the assumption that the Born cross section for the radiative process does not depend on energy.

The last 4 energy intervals listed in Table 1 are merged into 2 to increase statistics. The obtained values of 90% confidence level (CL) upper limits for 4 energy intervals are listed in Table 3.

7 Conclusion

In the experiment with the SND detector at the VEPP-2000 collider the cross section of the $e^+e^- \to \eta\eta\gamma$ process has been measured in the c.m. energy range from 1.17 to 2.00 GeV. The main intermediate mechanism in this energy range is $\phi\eta$. The measured $e^+e^- \to \eta\eta\gamma$ cross section is in good agreement with the CMD-3 measurement of the $e^+e^- \to \phi\eta$ process made in the $\phi \to K^+K^-$ decay channel. A search for contributions to the cross section from radiative processes has been carried out. No significant signal has been found. In the energy region corresponding to the resonances $\phi(1680)$ and $\rho(1700)$, the upper limit is 10.6 pb and significantly exceeds the estimates of the cross sections based on the predictions of Ref. [9] (see Sect. 1), $\sigma(e^+e^- \to \phi(1680) \to f_2'(1525)\gamma \to \eta\eta\gamma) = 1.7$ pb and $\sigma(e^+e^- \to \rho(1700) \to f_0(1500)\gamma \to \eta\eta\gamma) = 0.4$–$1.9$ pb.

Data Availability Statement This manuscript has no associated data or the data will not be deposited. [Authors' comment: All data are presented in the tables of the paper.]

Funded by SCOAP[3].

References

1. C. Edwards et al. (Crystal Ball Collaboration), Phys. Rev. Lett. **48**, 458 (1982)
2. M. Ablikim et al. (BESIII Collaboration), Phys. Rev. D **87**, 092009 (2013) [Erratum: Phys. Rev. D **87**, 119901 (2013)]
3. M.N. Achasov et al. (SND Collaboration), Phys. Atom. Nucl. **81**, 205 (2018)
4. V.L. Ivanov et al. (CMD-3 Collaboration), Phys. Lett. B **798**, 134946 (2019)
5. B. Aubert et al. (BaBar Collaboration), Phys. Rev. D **76**, 092005 (2007) [Erratum: Phys. Rev. D **77**, 119902 (2008)]
6. B. Aubert et al. (BaBar Collaboration), Phys. Rev. D **77**, 092002 (2008)
7. M. Ablikim et al. (BESIII Collaboration), Phys. Rev. D **104**, 032007 (2021)
8. A. Donnachie, Y.S. Kalashnikova, Phys. Rev. D **60**, 114011 (1999)
9. F.E. Close, A. Donnachie, Y.S. Kalashnikova, Phys. Rev. D **65**, 092003 (2002)
10. P.A. Zyla et al. (Particle Data Group), Rev. Part. Phys. PTEP **2020**, 083C01 (2020)
11. M.N. Achasov et al., Nucl. Instrum. Methods A **598**, 31 (2009)
12. V.M. Aulchenko et al., Instrum. Methods A **598**, 102 (2009)
13. A.Yu. Barnyakov et al., Nucl. Instrum. Methods A **598**, 163 (2009)
14. V.M. Aulchenko et al., Nucl. Instrum. Methods A **598**, 340 (2009)
15. P.Y. Shatunov et al., Status and perspectives of the VEPP-2000. Phys. Part. Nucl. Lett. **13**, 995 (2016)

16. E.A. Kuraev, V.S. Fadin, Sov. J. Nucl. Phys. **41**, 466 (1985) [Yad. Fiz. **41**, 733 (1985)]
17. G. Bonneau, F. Martin, Nucl. Phys. B **27**, 381 (1971)
18. S. Agostinelli et al. (GEANT4 Collaboration), Nucl. Instrum. Methods A **506**, 250 (2003)
19. M.N. Achasov et al. (SND Collaboration), Eur. Phys. J. C **80**, 1008 (2020)
20. A.V. Bozhenok, V.N. Ivanchenko, Z.K. Silagadze, Nucl. Instrum. Methods A **379**, 507 (1996)
21. J.P. Lees et al. (BaBar Collaboration), Phys. Rev. D **97**, 052007 (2018)
22. M.N. Achasov et al. (SND Collaboration), Phys. Rev. D **99**, 112004 (2019)
23. G. Cowan, K. Cranmer, E. Gross, O. Vitells, Eur. Phys. J. C **71**, 1554 (2011) [Erratum: Eur. Phys. J. C **73**, 2501 (2013)]
24. M.N. Achasov et al. (SND Collaboration), Phys. Rev. D **88**, 054013 (2013)
25. M.N. Achasov et al. (SND Collaboration), Phys. Rev. D **94**, 112001 (2016)
26. A.L. Read, J. Phys. G **28**, 2693 (2002)
27. T. Junk, Nucl. Instrum. Methods A **434**, 435 (1999)